C. R. Mecanique 340 (2012) 420–433

Contents lists available at SciVerse ScienceDirect

Comptes Rendus Mecanique

www.sciencedirect.com

Scaling of statistics in wall-bounded turbulent flows

Lois d'échelle des moments statistiques pour des écoulements turbulents pariétaux

L. Keirsbulck [a,b], G. Fourrié [a,b], L. Labraga [a,b], M. Gad-el-Hak [c,*]

[a] *Univ. Lille Nord de France, 59000 Lille, France*
[b] *UVHC, TEMPO, 59313 Valenciennes, France*
[c] *Department of Mechanical & Nuclear Engineering, Virginia Commonwealth University, Richmond, VA 23284-3015, USA*

ARTICLE INFO

Article history:
Received 10 January 2012
Accepted after revision 22 February 2012
Available online 16 March 2012

Keywords:
Turbulence
Wall-bounded flows
LDA & HWA measurements
Scaling

Mots-clés :
Turbulence
Écoulements turbulents pariétaux
Mesures anémométriques laser et fil chaud
Lois d'échelle

ABSTRACT

High-resolution laser Doppler anemometry (LDA) and hot-wire anemometry (HWA) measurements are utilized to study a zero-pressure-gradient turbulent boundary layer over the range of momentum thickness Reynolds number of 1170–3720. The primary objective is to investigate the near-wall behavior of this type of flow. We are particularly interested in possible Reynolds- and Kármán-number dependencies. The experimental results are in excellent agreement with most recent direct numerical simulations (DNS), which allow direct comparison of detailed results such as peak value and position of streamwise Reynolds stress, wall values of skewness and flatness factors, and turbulence dissipation rate. Systematic changes of some of these parameters with Kármán number are found when scaled with the inner parameters. A remedy seems to be the alternative mixed scaling that is based on $u_\tau^{3/2}U_0^{1/2}$, instead of u_τ^2, which admits direct influence of the outer velocity scale on the wall parameters.

RÉSUMÉ

Des mesures d'anémométrie laser (LDV) et fil chaud haute résolution ont été utilisées pour étudier la couche limite turbulente sans gradient de pression pour des nombres de Reynolds, basés sur l'épaisseur de quantité de mouvement, compris entre 1170 et 3720. L'objectif de cette étude vise à analyser le comportement de cet écoulement en région de proche paroi. Nous nous sommes particulièrement intéressés à une éventuelle dépendance vis-à-vis des nombres de Reynolds et de Kármán. Les résultats expérimentaux sont en excellent accord avec les simulations numériques directes (DNS) les plus récentes, ce qui permet une comparaison fine avec certaines quantités telles la valeur et la position du maximum de la tension de Reynolds, les facteurs de dissymétrie et d'aplatissement en région de proche paroi et le taux de dissipation turbulente. Une dépendance systématique au nombre de Kármán de ces quantités est observée lorsque l'adimensionnement en variables internes est utilisé. Une alternative possible consiste à utiliser des variables mixtes basées sur $u_\tau^{3/2}U_0^{1/2}$ plutôt que sur u_τ^2, celles-ci présentant l'avantage de prendre en compte les échelles externes dans l'adimensionnement des paramètres pariétaux.

* Corresponding author.
E-mail address: gadelhak@vcu.edu (M. Gad-el-Hak).

1631-0721/$ – see front matter
doi:10.1016/j.crme.2012.02.005

1. Introduction

The subject of wall-bounded turbulence has received an increasing attention over the past decades [1,2]. Important foci of research have always been the structure and scaling of this specific flow even in its canonical form [3]. However, despite extensive studies on zero-pressure-gradient boundary layers, and pressure-driven pipe and channel flows, crucial questions with respect to the scaling of mean flow, Reynolds stresses and higher-order moments remained. Experimental and numerical observations indicate that many of these statistical properties are very similar close to the wall, even though the small-scale structures there are modulated differently in different flow geometries by outer large-scale structures [4]. Therefore, high-resolution experiments in conjunction with the search for Reynolds-number similarities are an essential concept to investigate the fundamental properties of such behavior.

The classical view assumes a physical structure formally describing two separate scaling regions consisting of disparate sets of characteristic scales for velocity, length and time. While there is consensus about the characteristic inner scales, which are the friction velocity u_τ, the viscous length scale ν/u_τ, and the characteristic time ν/u_τ^2, the outer scales are still the subject of controversy. For the most part, the velocity at the outer edge of the boundary layer or at the centerline of a pipe or channel, U_0, is assumed to be the characteristic velocity scale. As characteristic length, the boundary-layer thickness, channel half-width or pipe radius, δ, momentum thickness, δ_θ, or Rotta–Clauser boundary-layer thickness, $\Delta = \int (U_0 - U)/u_\tau \, \mathrm{d}y$, is used [1,5,6].

In a recent paper [7], the different scaling concepts including classical, mixed and outer scaling were investigated in detail. This study primarily employed the Kármán number, defined as $Re_\tau = u_\tau \delta/\nu$. The authors argued that this ratio of outer- and inner-length scales is the proper similarity number upon which near-wall behavior should depend. This argument is strongly supported by Marusic et al. [8] who developed a model to calculate the streamwise near-wall turbulence based only on large-scale information from the logarithmic region.

The observed dependency of the stresses on the Kármán number can be reduced to a large extent when shifting to mixed scaling. This scaling is based on $u_\tau^{2-\alpha} U_0^\alpha$, instead of u_τ^2. Several attempts have been made to determine an optimum exponent α. The best known was presented by DeGraaff and Eaton [9] who set α equal to unity. In general, no physical or mathematical argument exists thus far to derive α directly. Therefore, the value of α is empirically determined. Buschmann et al. [7] found from an extensive analysis of DNS and experimental results an α-value of 1/2. To distinguish the scaling based on $\alpha = 1/2$ from the mixed scaling based on $\alpha = 1$ by DeGraaff and Eaton [9], Buschmann et al. [7] named their approach 'alternative mixed scaling'.

Beside theoretical considerations, precise physical experiments are still the silver bullet to gain insight into flow physics. A survey of recent wall measurements [10,11,9,12–14] brings to light that most intensive experimental investigations of the streamwise fluctuations have been conducted. With respect to scaling issues, determination of wall-skin friction and probe resolution closest to the wall are crucial [15]. The present study takes both issues into account and provides a high-resolution experimental data set of a fully-developed, zero-pressure-gradient turbulent boundary layer (abbreviated henceforth as ZPG TBL). Additionally, we compare our results with several direct numerical simulation studies and the alternative mixed scaling approaches proposed by Buschmann et al. [7].

2. Experimental approach

2.1. Facilities and experiments

The experiments took place in the horizontal, closed-loop, subsonic wind tunnel of Laboratoire TEMPO at Université de Valenciennes. The test section is 10 m long with a cross-section of 2×2 m^2. The facility is described in detail in Fourrié et al. [16]. The fully-developed turbulent boundary layer was measured on the lower floor of the wind tunnel, along the centerline of the test section. The measurements were carried out 9 m from the leading edge of the floor of the wind tunnel, and therefore no special techniques were needed to trip the boundary layer. The wind tunnel has a constant cross-section, so the boundary-layer growth resulted in a slight favorable pressure gradient. However, the corresponding acceleration parameter defined as

$$K = \frac{\nu}{U_0^2} \frac{\mathrm{d}U_0}{\mathrm{d}x} \tag{1}$$

shows that the acceleration is negligible (Table 1). Note that substantial deviation from the classical logarithmic law occurs for $K > 1.0\text{–}1.6 \times 10^{-6}$, a range that the present experiments stayed well below [17,18].

Details of the experimental conditions are summarized in Table 1. For all test cases, the freestream normal stress was less than 0.5%. Measurements were made at several wall-normal positions through viscous and classical logarithmic regions, with both LDA and HWA measuring techniques. The boundary-layer thickness δ was determined from the mean-velocity profiles at $0.99U_0$, where U_0 denotes the freestream velocity. The friction velocity u_τ is obtained according to the viscous sublayer law directly via a fit of the near-wall LDA data.

Table 1
Parameters of ZPG TBL studied. The following parameters are given in wall units: l^+ (hot-wire length), d_y^+ (LDA-measurement volume), and y_{min}^+ (LDA position closest to the wall). All other variables are defined in the text.

U_0 (m s^{-1})	$K \times 10^6$	u_τ (m s^{-1})	Re_θ	Re_τ	l^+	d_y^+	y_{min}^+	Symbol
0.68	0.397	0.032	1170	410	2.66	0.213	0.74	circle
0.88	0.356	0.040	1430	490	3.34	0.267	0.55	down triangle
1.15	0.318	0.052	1770	600	4.34	0.347	0.19	up triangle
2.20	0.151	0.094	2980	960	7.84	0.627	0.32	square
2.90	0.094	0.120	3720	1170	10.00	0.800	0.47	diamond

2.2. Hot-wire anemometry setup

A standard Dantec 55P15 miniature boundary-layer probe made of platinum-plated tungsten wire, in conjunction with a Dantec StreamLine hot-wire anemometer unit in the constant-temperature mode, was employed for measuring the u-component. The diameter of the hot-wire is 5 μm, and its length is 1.25 mm. The overheat ratio was set to 1.8 throughout the entire investigation. The hot-wires were calibrated in the freestream using a Prandtl tube immediately before every set of measurements. The probe was calibrated using several runs to verify the calibration accuracy. Exclusion of the near-wall region during the hot-wire measurements allowed the velocity range over which the calibration has to be carried out to be kept reasonably small. The main advantage of this strategy is that the calibration could be made with accuracy. The probe was mounted at a right-angle support attached to a traverse gear. Traversing resolution in the wall-normal direction is 10 μm.

Based upon a study involving different facilities and measurement techniques, Alfredsson et al. [10] already showed that a wire length less than 6 viscous units is required to capture the large velocity fluctuations corresponding to $u'/U = 0.4$ in the viscous sublayer. Here u' denotes the root-mean-square value of the streamwise velocity fluctuations and U the local mean velocity in the streamwise direction. Similarly, an attenuation in the near-wall peak of the streamwise normal stress in inner variables ($u'^+ = u'/u_\tau$) up to 30–40% depending on the wire length can be noticed. Based on high-resolution hot-wire measurements over a wide range of Kármán number up to $Re_\tau \approx 1800$, Metzger and Klewicki [19] and DeGraaff and Eaton [9] estimated that probe scales less than 10 viscous units are required to capture the proper Reynolds-number dependence in the peak value of u'^+, which is in agreement with the HWA results of Ligrani and Bradshaw [20] and Hutchins et al. [15]. In our case, the ratio of the active length to the diameter of the wires, l/d, was approximately 250, and the largest non-dimensionalized wire length was around 10 wall units (see Table 1).

2.3. LDA equipment and near-wall correction

A one-component LDA system was mounted on the same traverse as the HWA device. The LDA is composed of Dantec fiberoptic-based optics and the accompanied electronics. The system has a backscatter diffusion, the only optical configuration possible for measurements very close to a solid wall. The laser is a 250 mW Flowlite model. Beam splitting and frequency shifting are provided by Dantec Fiber flow optics. Signal processing is accomplished via a DANTEC BSA Flow software. An oil droplet generator (9307 TSI atomizer) was employed to generate the seeding for the LDA measurements. Mean diameter of seeding particles is approximately 1 μm.

One of the aims of the present experiments was to obtain highly accurate LDA measurement of near-wall turbulence and to compare these data directly with corresponding DNS results. In order to achieve a sufficient quality for the turbulence statistics, each measurement was taken with an integration time of 300 s. Uncertainties in the near-wall LDA measurements arise from the random motion of the seed particles due to the finite sample size, and from systematic errors caused by velocity bias as well as the finite extent of the measuring volume. Random errors were negligible, but affect the precision of the higher-order moments very close to the wall. This is because of the infrequent arrival of seed particles in the near-wall region, which requires unrealistically large integration time.

The main uncertainties of the LDA technique due to velocity bias and velocity-gradient broadening have been discussed in the standard literature [11,21]. The bias uncertainty for the mean velocity was estimated to be less than 0.5%, and the velocity-gradient error must be considered and corrected in the thin near-wall region. Indeed, owing to the spatial distribution of the turbulence fluctuations, the Doppler-shift frequency obtained from each scattering particle did not correspond to the velocity in the center of the measuring control volume, but rather represented time- and volume-integrated information. Particularly very close to the wall, the measured turbulence properties showed a dependence on the size of the measuring control volume and required therefore a volume correction. Although the minor axis of the control volume, d_y^+, was small (see Table 1), this correction was necessary to obtain the appropriate accuracy. For this purpose, the spatial integration of the LDA signals due to the finite size of the measuring control volume was derived analytically to yield explicit relationships between measured mean quantities and the time-averaged local value at the center of the measuring control volume [11,22]. The mean and the fluctuating parts of the velocity are expanded in Taylor series

$$U_i = U_{i,c} + \sum_{n=1}^{\infty} \frac{1}{n!} \left(\frac{\partial^n U_i}{\partial x_j^n} \right)_c (x_j - x_{j,c})^n \tag{2}$$

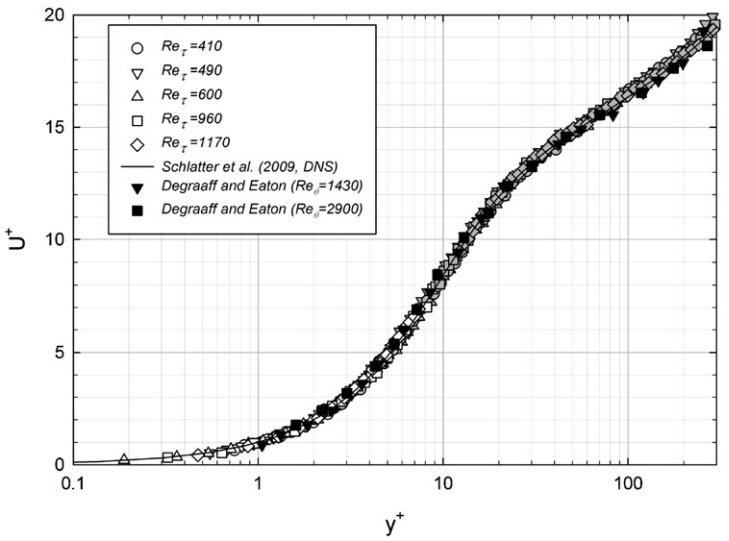

Fig. 1. Mean-velocity profiles as a function of inner-normalized position above the surface. LDA measurements (open symbols), HWA measurements (gray symbols), DNS from Schlatter et al. [23] (solid line) and LDA measurements from DeGraaff and Eaton [9] (black symbols).

$$u_i = u_{i,c} + \sum_{n=1}^{\infty} \frac{1}{n!} \left(\frac{\partial^n u_i}{\partial x_j^n} \right)_c (x_j - x_{j,c})^n \tag{3}$$

A volume- and time-integration procedure [11] yields the following corrections for the mean velocity and the turbulence normal stress

$$U_c^+ \approx U_{cv}^+ - \frac{\tilde{d}_y^{+2}}{32} \left(\frac{\partial^2 U^+}{\partial y^{+2}} \right)_c + \text{h.o.t.} \tag{4}$$

$$u_c'^2 \approx u_{cv}'^{+2} - \frac{\tilde{d}_y^{+2}}{16} \left(\frac{\partial U^+}{\partial y^+} \right)_c^2 + \text{h.o.t.} \tag{5}$$

where $\tilde{d}_y^+$ denotes the non-dimensionalized extent of the measuring volume, defined on the basis of the minimum detectable signal level. Subscript c denotes the center of the volume and subscript cv denotes time- and volume-integrated information. These formulas were used to correct all wall measurements. The measured mean velocity is very close to the time-averaged value at the center of the measuring control volume since the correction depends only on the second derivative of the mean-velocity profile, which is negligible close to the wall. Since the mean gradient is known accurately, this effect can be corrected. The gradient bias corrections were only applied for u'^2. In the near-wall region, below $y^+ \approx 2$, the lack of sufficient samples leads to a large scattering of data especially for the high-order statistical moments. Therefore the gradient bias correction was not applied to the skewness and flatness factors.

3. Results and discussion

3.1. Streamwise mean velocity

Fig. 1 presents the mean-velocity profiles in comparison with the DNS results from Schlatter et al. [23] and experimental data from DeGraaff and Eaton [9]. Both LDA and HWA measurements are in very good agreement with the DNS and experimental data.

HWA measurements within the viscous sublayer are known to be strongly affected by the wall [24]. Because LDA measurements are non-intrusive and free of heat-conduction effects, they are therefore the preferred experimental technique in this region. A closeup view of our LDA profiles is shown in Fig. 2. The near-wall profiles are in excellent agreement with the theoretically predicted linear velocity distribution up to $y^+ \approx 4$, which is also confirmed by Schlatter's DNS data. Following Monin and Yaglom [25], the near-wall profile can be expanded in a Taylor series

$$U^+ = y^+ + \sum_{i=4}^{\infty} a_i y^{+i} \tag{6}$$

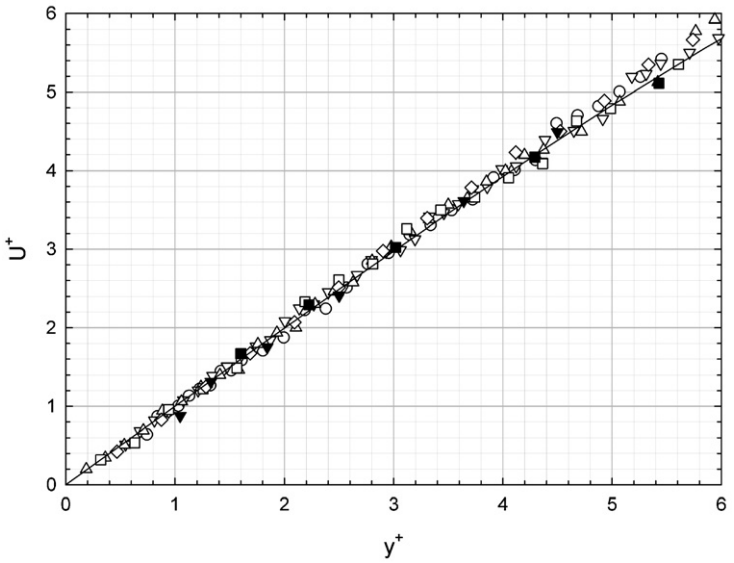

Fig. 2. Closeup view of LDA mean-velocity profiles. Symbols are the same as in Fig. 1.

Fitting the LDA data ($0 \leqslant y^+ \leqslant 8.5$), an averaged nearly Reynolds-number-independent value of $a_4 = -1.90 \times 10^{-4}$ is obtained for $Re_\tau \geqslant 600$. This value is in good agreement with $a_4 = -1.88 \times 10^{-4}$ obtained from an equivalent fit of Schlatter's DNS.

3.2. Behavior of streamwise normal stress near the wall

Much work has been devoted to the understanding of the structure of wall turbulence. One of the outcomes is that the ratio u'^+/U^+ at the wall seems to have an asymptotic value of about 0.4 for sufficiently high Reynolds numbers [26–28]. It is worthwhile to analyze this ratio and its Reynolds-number dependency in detail, since it sheds some light on the dynamics of turbulence in the near-wall region. Again, we follow the textbook by Monin and Yaglom [25] and write a Taylor series for the streamwise fluctuations

$$u'^+ = \sum_{i=1}^{\infty} b_i^+ y^{+i} \tag{7}$$

The wall value of the sought ratio is closely related to the ratio of the wall-shear-stress fluctuations to the wall-shear stress itself and follows from dividing the first-order terms of Eq. (7) and Eq. (6)

$$\tau_{w,rms}^+ = \frac{\tau_w'}{\tau_w} = \lim_{y^+ \to 0} \frac{u'^+}{U^+} = b_1^+ \tag{8}$$

A closeup view of the streamwise Reynolds stress in the viscous sublayer is shown in Fig. 3. Again, the measurements are in good agreement with Schlatter's DNS data and the experimental results by DeGraaff and Eaton [9]. A comparison with the first term of the Taylor series, Eq. (7), around $y^+ = 0$ ($b_1^+ = 0.4$) shows a reasonable concordance with the LDA data up to $y^+ \approx 3.0$–3.5, which is in agreement with Buschmann et al. [7]. The high reliability of the obtained data is further supported by their representation in Fig. 4, where the relative level of the near-wall streamwise velocity fluctuations is plotted against the normalized wall-normal coordinate. Such a representation is very sensitive to the accuracy of the measurements, since it emphasizes the measuring errors that usually increase within the viscous sublayer.

The limiting behavior of the streamwise normal stresses near the wall ($y^+ < 4$) reproduced from various experimental and numerical studies is given in Fig. 5.

Both numerical and experimental data reveal similar trends. With increasing Kármán number, an asymptotic value of about 0.40–0.43 is approached. However, the DNS ZPG TBL results exhibit a slightly higher value than the experimental results. Similar tendencies were already observed by Fischer et al. [27]. Additional differences between confined and semi-confined flows may exist as the DNS data show in the lower Kármán-number range. According to Fischer et al. [27], the asymptotic expansion for the limiting behavior of the streamwise normal stresses near the wall is written as follows:

$$b_1^+ = b_{1,0}^+ + \frac{b_{1,1}^+}{Re_\tau} + \frac{b_{1,2}^+}{Re_\tau^2} + \text{h.o.t.} \tag{9}$$

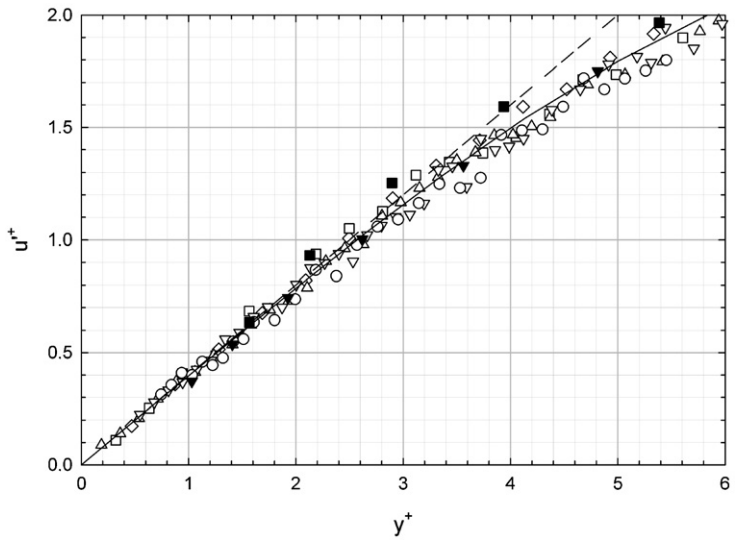

Fig. 3. Closeup view of u' LDA data. Black symbols are from DeGraaff and Eaton [9], all other symbols are the same as in Fig. 1. Dashed line represents the expansion series $u'^{+} = 0.4y^{+}$.

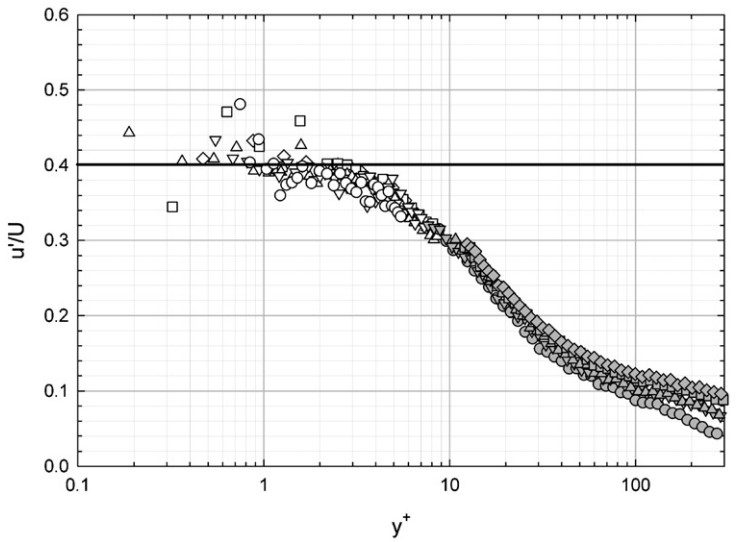

Fig. 4. Limiting behavior of streamwise normal stress near wall at different Kármán numbers. Symbols are the same as in Fig. 1.

The leading-order term represents the inviscid limit for $Re_\tau \to \infty$. The Reynolds-number effects are taken into account by the higher-order terms of the reciprocals of powers of the Kármán number. Confined and semi-confined DNS data fits lead to an inviscid asymptotic value of 0.432. However, fits of the experimental data deliver smaller values (see insert Fig. 5). The main reason for this systematic departure is that DNS data reach closer to the wall ($y^+_{min} \approx 0.03$–0.04) than experimental results (this work $y^+_{min} \approx 0.2$–0.7). However, the change of the Re_τ-dependency over this y^+-region should be minute. Therefore, the gradient of the fits of numerical and experimental values should be similar, which is clearly the case as the higher-order terms of Eq. (9) indicate.

Another reason for the difference is the electronic noise level induced by the experimental environment, which can be relatively important close to the wall. The slope of the streamwise normal stress would then be slightly under-estimated. A third possibility is that several DNS results might be biased by too short computation domains, as pointed out by Chin et al. [29]. Therefore, direct measurement of the wall-shear stress is needed. The present authors recently conducted such experiments in a turbulent channel flow using the electrochemical method [30]. The results are in good agreement with those numerically obtained using DNS. However, none of these arguments seems to explain the separation of the transitional ZPG TBL DNS by Wu and Moin [31], which has already been noted by Örlü and Schlatter [32].

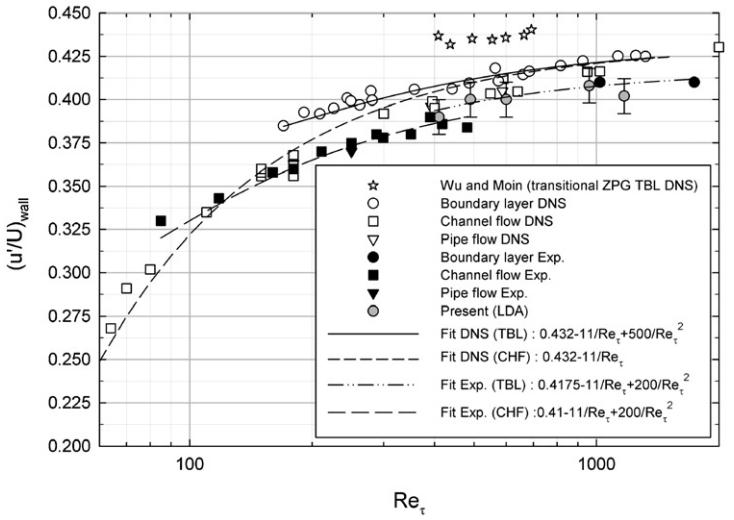

Fig. 5. Relative intensity of streamwise velocity fluctuations as a function of Kármán number for the different authors listed in Table 2.

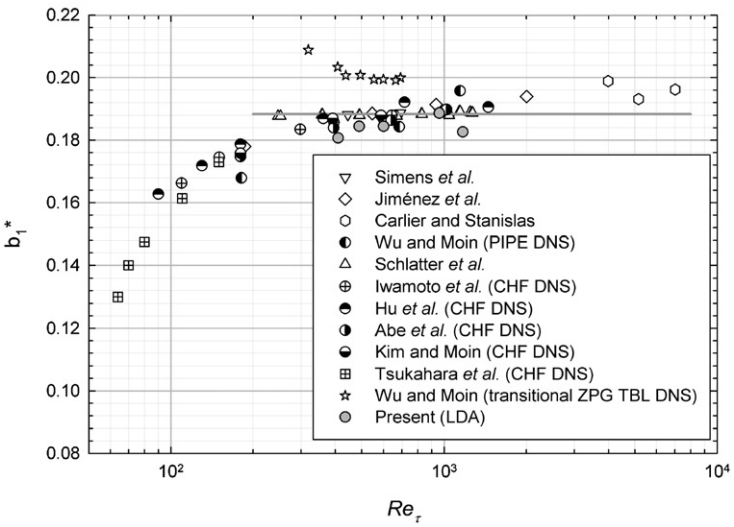

Fig. 6. Relative intensity of streamwise velocity fluctuations employing alternative mixed scaling. Data from the different authors listed in Table 2. Gray bold line indicates general trend of the ratio u'^*/U^+.

The observed dependency on the Kármán number can be removed to a large extent when shifting to an alternative mixed scaling [7]. Such scaling is based on $u_\tau^{3/2}U_0^{1/2}$ instead of on u_τ^2, so that the streamwise stress becomes

$$u'^* = u'^+ \frac{u_\tau^{1/4}}{U_0^{1/4}} = \sum_{i=1}^{\infty} b_i^* y^{+i} \tag{10}$$

Compared with the mixed scaling proposed by DeGraaff and Eaton [9], the influence of the outer characteristic velocity is weaker here. The ZPG TBL DNS data by Schlatter et al. [23] show a Kármán-number-independent value of $b_1^* = 0.1883$, which is confirmed by the data from Simens et al. [33] ($Re_\tau = 445$–690, $b_1^* = 0.1882$) and Lee and Sun [34] ($Re_\tau = 490$–827, $b_1^* = 0.1882$). Due to the reasons mentioned above, our experimental value $b_1^* = 0.1842$ is found slightly below the numerical results. Fig. 6 clearly reveals that all b_1^*-values independent of the flow configuration aspire to a constant value above $Re_\tau \approx 400$. Again the DNS by Wu and Moin [31] make an exception. Obviously the departure of $\tau_{w,rms}^+$ of this specific DNS is resistant to any scaling argument.

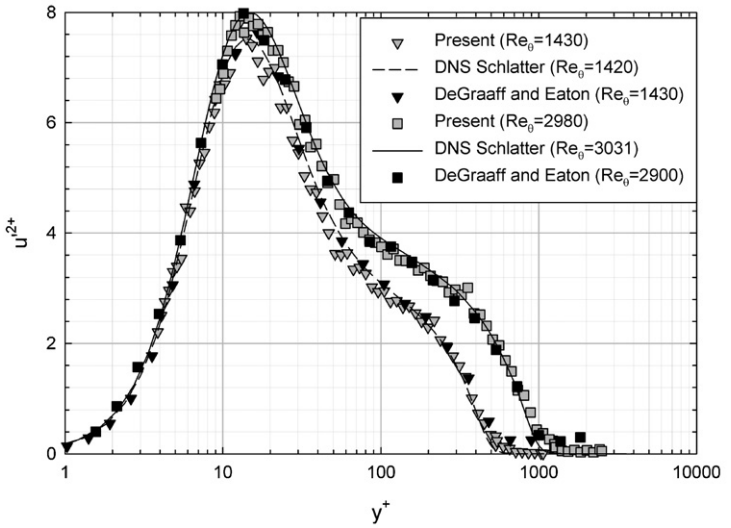

Fig. 7. Comparison of experimental and numerical streamwise normal stresses with present HWA measurements. Black symbols are from DeGraaff and Eaton [9], all other symbols are the same as in Fig. 1.

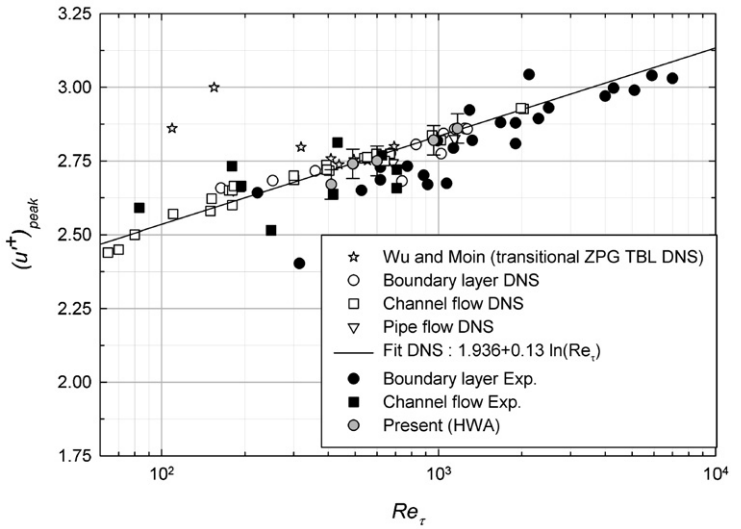

Fig. 8. Variation of the peak value of the inner-scale streamwise normal stress with Kármán number. Symbols are the same as in Fig. 5.

3.3. Scaling of the streamwise normal stress

The streamwise normal stress is shown in Fig. 7. Reynolds-number effects are already visible with the unaided eye in the region above $y^+ = 8$. Once again, there is an excellent agreement with the experimental data by DeGraaff and Eaton [9] and the DNS by Schlatter et al. [23]. As already noticed by several authors (see, e.g., [1,12]), simple inner scaling based on u_τ alone is not sufficient to collapse characteristic parameters such as the peak value. In Fig. 8, we repeat Fig. 5 of Marusic et al. [1] but additionally add our own data. This representation confirms once again the failure of the classical inner scaling.

Remedies were proposed among others by DeGraaff and Eaton [9] with the standard mixed scaling and by Buschmann et al. [7] with the alternative mixed scaling. Herein we concentrate on the latter and plot in Fig. 9 the peak values of the streamwise stress from the data sets of Table 2. Above $Re_\tau \approx 100$, the peak values now show a Kármán-number-independent value of about 1.64. The averaged experimental value of this work is $\overline{u'^*_{max}} = 1.6057$ which is in excellent agreement with corresponding numerical results of Schlatter et al. [23] ($\overline{u'^*_{max}} = 1.5961$), of Simens et al. [33] ($\overline{u'^*_{max}} = 1.6073$), of Lee and Sun [34] ($\overline{u'^*_{max}} = 1.5913$) and the experiments by Osaka et al. [35] ($\overline{u'^*_{max}} = 1.5628$) and Carlier and Stanislas [36] ($\overline{u'^*_{max}} = 1.6764$). The differences between different flow geometries are nearly completely removed employing alternative scaling. Interestingly enough, the peak position of the streamwise stress does not need such a change in scaling (see Fig. 10).

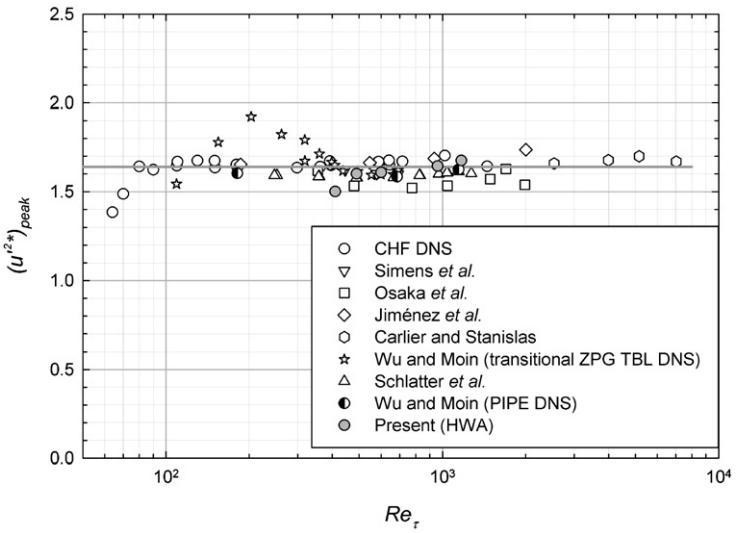

Fig. 9. Variation of the peak value of streamwise normal stress with Kármán number employing alternative mixed scaling. Data from the different authors listed in Table 2. Gray bold line indicates general trend of peak value.

Table 2
Data sets compiled for analysis. CHF indicates channel-flow data.

Authors	Flow	Technique	Authors	Flow	Technique
Lee and Sun [34]	TBL	DNS	Wu and Moin [31]	PIPE	DNS
Schlatter et al. [23]	TBL	DNS	Ching et al. [37]	TBL	LDA
Simens et al. [33]	TBL	DNS	Johansson and Karlsson [38]	TBL	LDA
Spalart [39]	TBL	DNS	Balint et al. [40]	TBL	HWA
Wu and Moin [41]	TBL	DNS	Carlier and Stanislas [36]	TBL	HWA
Abe et al. [42]	CHF	DNS	DeGraaff and Eaton [9]	TBL	HWA
Antonia and Kim [43]	CHF	DNS	Ligrani and Bradshaw [20]	TBL	HWA
DelÁdamo and Jiménez [44]	CHF	DNS	Osaka et al. [35]	TBL	HWA
Günther et al. [45]	CHF	DNS	Purtell et al. [46]	TBL	HWA
Hoyas and Jiménez [47]	CHF	DNS	Ueda and Hinze [48]	TBL	HWA
Iwamoto et al. [49]	CHF	DNS	Fischer et al. [27]	CHF	LDA
Jiménez et al. [50]	CHF	DNS	Poggi et al. [51]	CHF	LDA
Lyons et al. [52]	CHF	DNS	Wei and Willmarth [53]	CHF	LDA
Mansour et al. [54]	CHF	DNS	Khoo et al. [55]	CHF	HWA
Moser et al. [56]	CHF	DNS	Durst et al. [11,22]	PIPE	LDA
Pallares and Grau [57]	CHF	DNS	Present	TBL	LDA, HWA
Tsukahara et al. [58]	CHF	DNS			

A constant value of $(y_u^+)_{peak} = 14.4$ is found above $Re_\tau \approx 100$. The flow geometry does not or at least very weakly affect the peak position.

To summarize, the streamwise-fluctuation data presented here are in good agreement with comparable experiments and confirm some most recent numerical results. The quality of the data allows to firmly proof the inadequacy of classical inner scaling for the streamwise velocity fluctuation. It is experimentally shown that the streamwise stress and its peak value are better represented when the alternative mixed scaling is used. For both parameters Kármán-number-independent values are obtained above $\delta^+ \approx 400$ and $\delta^+ \approx 100$ respectively.

3.4. Higher-order statistics

Reliable statistics of higher-order moments in the near-wall region are difficult to obtain because large samples are required. However, considering the long integration time used in the present experiments to collect the near-wall measurement, the skewness and flatness factors have high fidelity down to three wall units. Skewness and flatness factors, defined respectively as

$$S_u = \frac{\overline{u^3}}{u'^3}, \qquad F_u = \frac{\overline{u^4}}{u'^4} \tag{11}$$

are presented in Figs. 11 and 12. Good agreement is seen between the presented data, the measurements by DeGraaff and Eaton [9] and Smith [59] and the DNS by Schlatter et al. [23]. Across the entire flow field, the higher-order moments exhibit

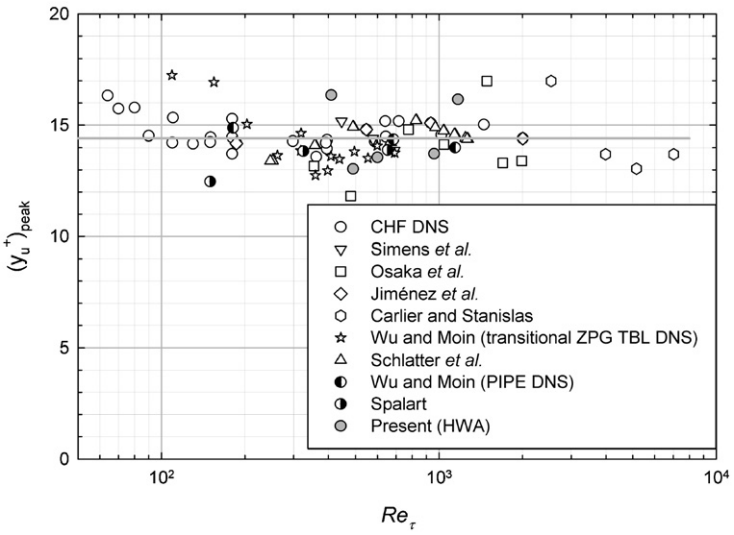

Fig. 10. Variation of the peak position of streamwise normal stress with Kármán number. Data from the different authors listed in Table 2. Gray bold line indicates general trend of peak position.

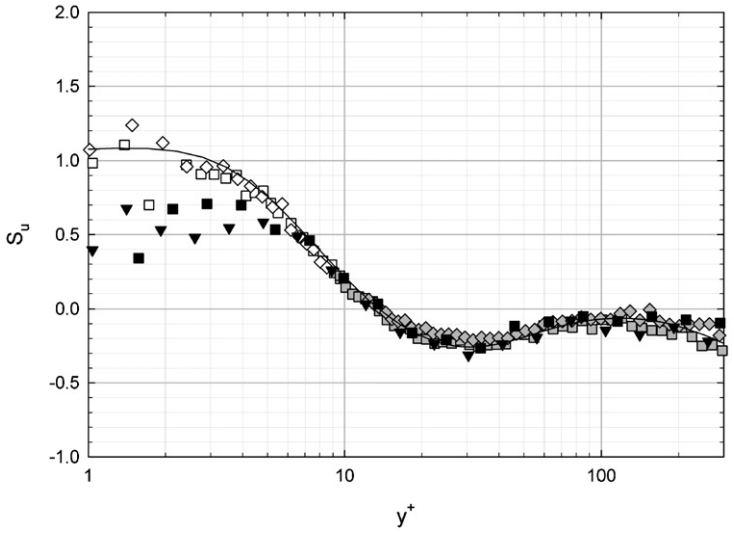

Fig. 11. Skewness factor of streamwise velocity fluctuations for $Re_\theta = 2980$ and 3720, compared to DNS. Symbols are the same as in Fig. 1.

a highly non-Gaussian character. In particular, the non-Gaussian variations are pronounced in the near-wall region. The sign of S_u is observed to change from a positive to a negative value at $y^+ \approx 12$.

Within the viscous sublayer, the present measurements are affected by the limited temporal resolution due to low data rates, even if the spatial resolution is satisfactory. However, the near-wall behavior is very similar to the DNS data. Both skewness and flatness factors exhibit limiting values close to 1 and 5, respectively. This confirms the accuracy of the near-wall measurements and the reliability of the DNS. Main statistics results obtained very close to the wall are reported in Table 3 and compared to the direct numerical simulations from Schlatter et al. [23] and Moser et al. [56]. It should be mentioned that for DNS data, the wall values of skewness and flatness were found to vary slightly as a function of Reynolds numbers. Hence, for Reynolds-number range close to the present measurements, both channel and boundary-layer numerical results are in excellent agreement.

3.5. Evaluation of the turbulence dissipation rate

Direct numerical simulations provide turbulence data very close to the wall. Such data are easily accessible for the calculation of spatial and temporal derivatives. This is especially true for the dissipation rate

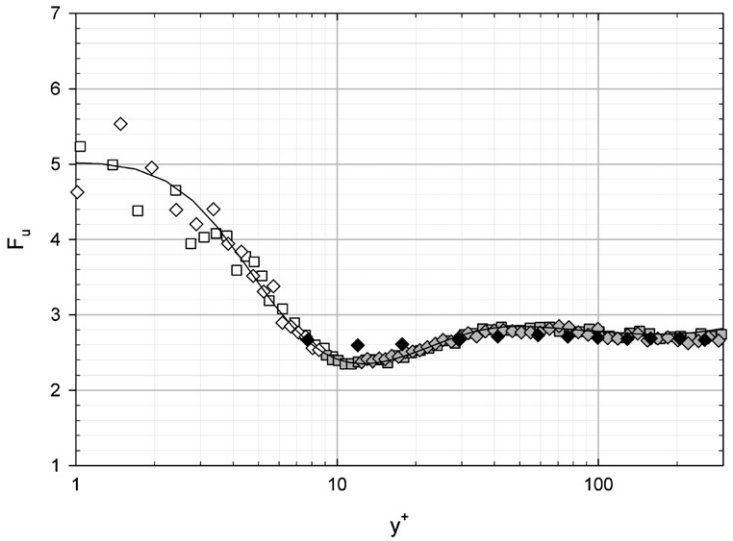

Fig. 12. Flatness factor of streamwise velocity fluctuations for $Re_\theta = 2980$ and 3720, compared to DNS. Black diamonds are from Smith [59]. Other symbols are the same as in Fig. 1.

Table 3
Statistics of streamwise velocity fluctuations at the wall.

Authors	Re_τ	Skewness	Flatness
Schlatter et al. [23]	492	0.98	4.71
Moser et al. [56]	587	1.02	4.87
Present	490	1.00	4.80

$$\varepsilon^+ = \overline{\frac{\partial u_i^+}{\partial x_k^+}\frac{\partial u_i^+}{\partial x_k^+}} \tag{12}$$

which is by definition based on spatial derivatives of the velocity fluctuations. Its estimation from experimental measurements is therefore rather complicated because some assumptions with respect to these derivatives are needed.

Different methods for the estimation of ε^+ employing single-component measurements have been proposed. Among them is Townsend's famous assumption [60] that turbulence dissipation and production of turbulence kinetic energy are approximately equal. Assuming further that the Reynolds shear stress is about u_τ^2, region of the classical log law is valid, the turbulence dissipation rate can be simplified as follows

$$\varepsilon^+ = -\overline{uv}^+\left(\frac{\partial U^+}{\partial y^+}\right) \approx \frac{1}{\kappa y^+} \tag{13}$$

which in turn gives the Kolmogorov's length scale as

$$\eta^+ = \left(\kappa y^+\right)^{1/4} \approx 0.8\left(y^+\right)^{1/4}; \quad \kappa = 0.41 \tag{14}$$

The simplified estimation for ε^+ follows from Kolmogorov's two similarity hypotheses for isotropic turbulence [61]. According to these hypotheses, the spectrum in the inertial subrange is only a function of the turbulence dissipation rate. The one-dimensional spectrum is then written as $E_{11} = C_1\varepsilon^{2/3}k_1^{-5/3}$. Here $C_1 \approx 0.49$ denotes the Kolmogorov constant [62]. In the present study, we obtain the dissipation rate by fitting the slope of the inertial subrange (Fig. 13).

The dissipation rates deduced from the two methods show reasonable agreement in the classical logarithmic region and slightly above it (Fig. 13). And indeed according to the classical view, the energy supplied by the turbulence kinetic energy cascades must be equal to the rate at which energy is dissipated by molecular viscosity. However, we have to note that serious doubts have recently been raised regarding applying the classical view to finite-Reynolds-number wall-bounded flows [63].

The last estimate employed allows the prediction of the turbulence dissipation rate at the wall. It is based on the idea of a limiting behavior of the turbulence time scale

$$t_w^+ = \lim_{y^+\to 0} k^{+2}/\left(y^{+2}\varepsilon^+\right) \tag{15}$$

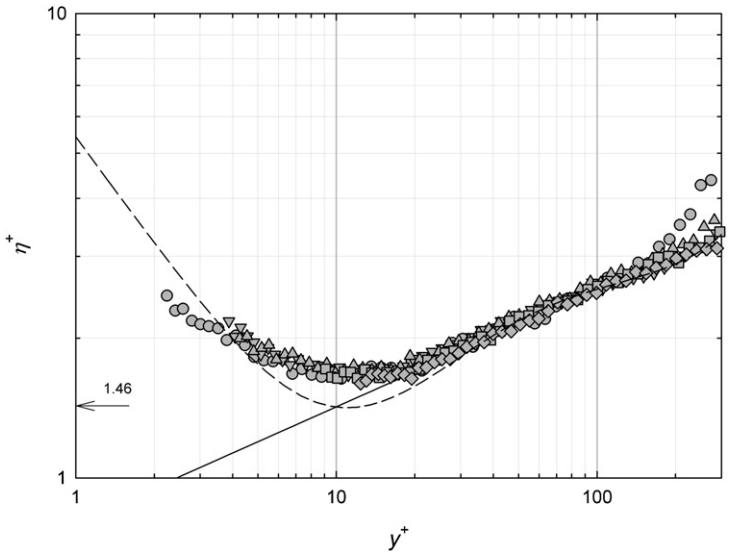

Fig. 13. Estimation of the Kolmogorov's length scale. Straight line denotes Townsend's assumption equation. Gray symbols denote the estimation of the turbulence dissipation rate based on the Kolmogorov's similarity hypothesis for the different Kármán numbers studied. Dashed line is from DNS results of Schlatter et al. [23].

Table 4
Percentage change between first and last values of the dissipation rate at the wall, for complete TKE.

Authors	Flow	Re_τ	Classical scaling	Alternative scaling
Schlatter et al. [23]	TBL	252–1271	19.68	6.29
Simens et al. [33]	TBL	445–690	6.08	1.88
Jiménez et al. [50]	CHF	186–2004	33.23	23.04
Hu et al. [65]	CHF	90–1451	48.96	40.47
Wu and Moin [31]	PIPE	181–1143	62.46	45.01

Table 5
Percentage change between first and last values of the dissipation rate at the wall, for incomplete TKE (based on u' alone).

Authors	Flow	Re_τ	Classical scaling	Alternative scaling
Schlatter et al. [23]	TBL	252–1271	13.80	1.06
Simens et al. [33]	TBL	445–690	4.83	0.58
Jiménez et al. [50]	CHF	186–2004	26.92	15.77
Hu et al. [65]	CHF	90–1451	37.41	27.00
Wu and Moin [31]	PIPE	181–1143	52.16	35.82
Osaka et al. [35]	TBL	355–1988	14.28	2.10
Present	TBL	410–1170	10.00	3.14

where k^{+2} denotes the turbulence kinetic energy, and ε^+ is the corresponding dissipation rate. Employing the Taylor series expansions of the velocity fluctuations [25] directly at the wall indicates that t_w^+ is identically one [43] and free of any Reynolds- or Kármán-number dependency. This allows the prediction of the wall dissipation rate directly from the limited behavior of the stress components [64].

Direct numerical simulations [66] show that the streamwise velocity component accounts for about 75% of the dissipation rate at the wall. Because our measurements are limited to this velocity component, we differentiate here between ε^+ based on the complete turbulence kinetic energy (TKE) and a reduced value of ε_u^+, where the TKE considers only the streamwise velocity component. From our data, we conclude that the turbulence dissipation rate and the Kolmogorov scale at the wall should have respectively averaged values of about

$$\varepsilon_{wu}^+ \approx 0.22; \qquad \eta_w^+ \approx 1.46 \tag{16}$$

However, the data show a weak but noticeable Kármán-number dependency, which again led to the idea of scaling the wall value of the turbulence dissipation rate employing the alternative mixed scaling proposed by Buschmann et al. [7]. The results are shown in Tables 4 and 5. Employing DNS data, the wall values of the dissipation rate based on the complete TKE indicate a significant decrease of the difference between first and last ε_w^+-value when alternative mixed scaling is employed instead of classical inner scaling. Interestingly enough, this decrease is much stronger for the ZPG TBL than for pipe and channel flows. Obviously we see here another facet of the difference between confined and semi-confined flows.

The observed effect is even more pronounced when it comes to wall values of the dissipation rate based on the reduced TKE (Table 5). Both numerical and experimental ZPG TBL indicate that there is nearly no change of the ε^+_{wu}-values during the development of the boundary layer. The differences between complete and reduced TKE can be explained by the different intensity of the outer large-scale motions modulate the fluctuations in the inner region.

4. Conclusions

In this article, a highly accurate set of near-wall data for flat-plate turbulent boundary layer is presented. Both LDA and HWA data confirm in excellent manner most recent DNS results [23]. This makes the experimental data particularly interesting for the validation of theoretical approaches. Herein we investigated especially mean flow, streamwise stress, skewness and flatness factors, and turbulence dissipation rate. Our results are summarized as follows:

(i) The coefficient of the second term of the viscous sublayer law is specified with $a_4 = -1.90 \times 10^{-4}$ for $y^+ \leqslant 8.5$. This value is nearly constant above $Re_\tau = 600$.
(ii) The relative intensity of the streamwise velocity fluctuations is a function of the Kármán number when scaled with inner variables. A Kármán-number-independent representation of experimental and numerical values is obtained when the alternative mixed scaling based on $u_\tau^{3/2} U_0^{1/2}$ is employed (Fig. 6).
(iii) In agreement with several other investigations, it is confirmed that the peak value of the streamwise stress depends strongly on Re_τ. However, applying alternative mixed scaling reduces this dependency. Differently, the peak position, $(y_u^+)_{peak}$, is best represented when employing classical inner scaling based on ν/u_τ, the viscous length scale.
(iv) Experimental skewness and flatness factors with high fidelity down to three wall units are presented and found to be in excellent agreement with DNS results. This is especially true for the obtained wall values, which closely resemble the numerical results (Table 3).
(v) An analysis of the turbulence dissipation rate based on different hypothesis indicates that in the classical logarithmic region and slightly above it, turbulence production and dissipation are balanced to first order. More detailed experiments are needed here to show that there are higher-order effects, and, as the case may be, how strong these are. With respect to the wall value of the dissipation rate, it is found that a nearly Re_τ-independent representation can be achieved when alternative mixed scaling is employed. However, it seems to be that even then significant differences between confined and semi-confined flows remain.

Acknowledgements

We are grateful to Dr. Matthias H. Buschmann from Institut für Luft- und Kältetechnik Dresden, Germany, for his helpful comments on this manuscript and for numerous discussions we had with him during the research. The present work has been supported by Campus International pour la Sécurité et l'Intermodalité des Transports, la Région Nord-Pas-de-Calais, l'Union Européenne, la Direction de la Recherche, Enseignement Supérieur, Santé et Technologies de l'Information et de la Communication et le Centre National de la Recherche Scientifique. The authors gratefully acknowledge the support of these institutions. We thank all scientists who supported us generously with their data.

References

[1] I. Marusic, B.J. McKeon, P.A. Monkewitz, H.M. Nagib, A.J. Smits, K.R. Sreenivasan, Wall-bounded turbulent flows at high Reynolds numbers: Recent advances and key issues, Phys. Fluids 22 (2010) 065103.
[2] J.C. Klewicki, Reynolds number dependence, scaling, and dynamics of turbulent boundary layers, J. Fluids Eng. 132 (2010) 1.
[3] R.L. Panton, Review of wall turbulence as described by composite expansions, Appl. Mech. Rev. 58 (2005) 1.
[4] R. Mathis, J.P. Monty, N. Hutchins, I. Marusic, Comparison of large-scale amplitude modulation in turbulent boundary layers, pipes, and channel flows, Phys. Fluids 21 (2009) 111703.
[5] P.A. Monkewitz, R.D. Duncan, H.M. Nagib, Correcting hot-wire measurements of stream-wise turbulence intensity in boundary layers, Phys. Fluids 22 (2010) 091701.
[6] H.H. Fernholz, P.J. Finley, The incompressible zero-pressure-gradient turbulent boundary layer: an assessment of the data, Prog. Aerospace Sci. 32 (1996) 245.
[7] M.H. Buschmann, T. Indinger, M. Gad-el-Hak, Near-wall behavior of turbulent wall-bounded flows, Int. J. Heat Fluid Flow 30 (2009) 993.
[8] I. Marusic, R. Mathis, N. Hutchins, Predictive model for wall-bounded turbulent flow, Science 329 (2010) 193.
[9] D.B. DeGraaff, J.K. Eaton, Reynolds-number scaling of the flat-plate turbulent boundary layer, J. Fluid Mech. 422 (2000) 319.
[10] P.H. Alfredsson, A.V. Johansson, J.H. Haritonidis, H. Eckelmann, The fluctuating wall-shear stress and the velocity field in the viscous sublayer, Phys. Fluids 31 (5) (1988) 1026.
[11] F. Durst, J. Jovanović, J. Sender, LDA measurements in the near-wall region of a turbulent pipe flow, J. Fluid Mech. 295 (1995) 305.
[12] J.F. Morrison, B.J. McKeon, W. Jiang, A.J. Smith, Scaling the streamwise velocity component in turbulent pipe flow, J. Fluid Mech. 508 (2004) 99.
[13] N. Hutchins, I. Marusic, Evidence of very long meandering features in the logarithmic region of turbulent boundary layers, J. Fluid Mech. 579 (2007) 1.
[14] M. Hultmark, S.C.C. Bailey, A.J. Smits, Scaling of near-wall turbulence in pipe flow, J. Fluid Mech. 649 (2010) 103.
[15] N. Hutchins, T.B. Nickels, I. Marusic, M.S. Chong, Hot-wire spatial resolution issues in wall-bounded turbulence, J. Fluid Mech. 635 (2009) 103.
[16] G. Fourrié, L. Keirsbulck, L. Labraga, P. Gilliéron, Bluff-body drag reduction using a deflector, Exp. Fluid 50 (2010) 385.
[17] V.C. Patel, Calibration of the Preston tube and limitations on its use in pressure gradients, J. Fluid Mech. 23 (1965) 185.
[18] W.P. Jones, B.E. Launder, The prediction of laminarization with two-equation model of turbulence, Int. J. Heat Mass Transfer 15 (2) (1972) 301.
[19] M.M. Metzger, J.C. Klewicki, A comparison study of near-wall turbulence in high and low Reynolds number boundary layer, Phys. Fluids 13 (3) (2001) 692.

[20] P.M. Ligrani, P. Bradshaw, Spatial resolution and measurement of turbulence in the viscous sublayer using subminiature hot-wire probes, Exp. Fluid 5 (1987) 407.
[21] D.A. Compton, J.K. Eaton, A high-resolution laser Doppler anemometer for three-dimensional turbulent boundary layers, Exp. Fluid 22 (1996) 111.
[22] F. Durst, H. Kikura, I. Lekakis, J. Jovanović, Wall shear stress determination from near-wall mean velocity data in turbulent pipe and channel flows, Exp. Fluid 20 (1996) 417.
[23] P. Schlatter, R. Örlü, Q. Li, G. Brethouwer, J.H. Fransson, A.V. Johansson, P.H. Alfredsson, D.S. Henningson, Turbulent boundary layers up to $Re_\theta = 2500$ studied through simulation and experiment, Phys. Fluids 21 (2009) 051702.
[24] P.V. Lanspeary, M.K. Bull, Correction of sublayer turbulence measurements for wall proximity effects in hot-wire anemometry, in: 11th Australasian Fluid Mechanics Conference, December 1992.
[25] A.S. Monin, A.M. Yaglom, Statistical fluid mechanics: mechanics of turbulence, in: J.L. Lumley (Ed.), English Translation, vol. 2, MIT Press, Cambridge, Massachusetts, USA, 1971.
[26] R. Örlü, J.H.M. Fransson, P.H. Alfredsson, On near wall measurements of wall bounded flows – the necessity of an accurate determination of the wall position, Prog. Aerospace Sci. 46 (8) (2010) 353.
[27] M. Fischer, J. Jovanović, F. Durst, Reynolds number effects in the near-wall region of turbulent channel flows, Phys. Fluids 13 (6) (2001) 1755.
[28] D.R. Chapmann, G.D. Kuhn, The limiting behaviour of turbulence near a wall, J. Fluid Mech. 170 (1986) 265.
[29] C. Chin, A.S.H. Ooi, I. Marusic, H.M. Blackburn, The influence of pipe length on turbulence statistics computed from direct numerical simulation data, Phys. Fluids 22 (2010) 61.
[30] L. Keirsbulck, L. Labraga, M. Gad el Hak, Statistical properties of wall-shear-stress fluctuations in turbulent channel flows, Int. J. Heat Fluid Flow (2012), in press.
[31] X. Wu, P. Moin, A direct numerical simulation study on the mean velocity characteristics in turbulent pipe flow, J. Fluid Mech. 608 (2008) 81.
[32] R. Örlü, P. Schlatter, On the fluctuating wall-shear stress in zero pressure-gradient turbulent boundary layer flows, Phys. Fluids 23 (2011) 021704.
[33] M.P. Simens, J. Jiménez, S. Hoyas, Y. Mizuno, A high-resolution code for turbulent boundary layers, J. Computat. Phys. 228 (11) (2009) 4218.
[34] J.H. Lee, H.J. Sun, Direct numerical simulation of a turbulent boundary layer up to $Re_\theta = 2500$, Int. J. Heat Fluid Flow 32 (2011) 1.
[35] H. Osaka, T. Kameda, S. Mochizuki, Re-examination of the Reynolds number effect on the mean flow quantities in a smooth wall turbulent boundary layer, JSME Int. J. 41 (1988) 123.
[36] J. Carlier, M. Stanislas, Experimental study of eddy structures in a turbulent boundary layer using particle image velocimetry, J. Fluid Mech. 535 (2005) 143.
[37] C. Ching, L. Djenidi, R. Antonia, Low-Reynolds-effects in a turbulent boundary layer, Exp. Fluid 19 (1995) 61.
[38] T. Johansson, R. Karlsson, The energy budget in the near-wall region of a turbulent boundary layer, in: R.J. Adrian, T. Asanuma, D.F.G. Durao, F. Durst, J.H. Whitelaw (Eds.), Applications of Laser Anemometry to Fluid Mechanics, Springer, 1989, p. 3.
[39] P.R. Spalart, Direct simulation of a turbulent boundary layer up to $Re_\theta = 1410$, J. Fluid Mech. 187 (1988) 61.
[40] J.L. Balint, J.M. Wallace, P. Vukoslavcevic, The velocity and vorticity vector fields of a turbulent boundary layer. Part 2. Statistical properties, J. Fluid Mech. 228 (1991) 53.
[41] X. Wu, P. Moin, Direct numerical simulation of turbulence in a nominally zero-pressure-gradient flat-plate boundary layer, J. Fluid Mech. 630 (2009) 5.
[42] H. Abe, H. Kawamura, H. Choi, Very large-scale structures and their effects on the wall shear-stress fluctuations in a turbulent channel flow up to $Re_\tau = 640$, Phys. Fluids 126 (2004) 835.
[43] R.A. Antonia, J. Kim, Low-Reynolds-number effects on near-wall turbulence, J. Fluid Mech. 276 (1994) 61.
[44] J.C. DelÁdamo, J. Jiménez, Spectra of the very large anisotropic scales in turbulent channels, J. Fluid Mech. 500 (2004) 135.
[45] A. Günther, D.V. Papavassiliou, M.D. Warholic, T.J. Hanratty, Turbulent flow in a channel at low Reynolds number, Exp. Fluid 25 (1998) 503.
[46] P. Purtell, P. Klebanoff, F. Buckley, Turbulent boundary layer at low Reynolds number, Phys. Fluids 24 (1981) 802.
[47] S. Hoyas, J. Jiménez, Scaling of the velocity fluctuations in turbulent channels up to $Re_\tau = 2003$, Phys. Fluids 18 (2006) 011702.
[48] H. Ueda, J.O. Hinze, Fine-structure turbulence in the wall region of a turbulent boundary layer, J. Fluid Mech. 67 (1975) 125.
[49] K. Iwamoto, Y. Suzuki, N. Kasagi, Reynolds number effect on wall turbulence: Toward effective feedback control, Int. J. Heat Fluid Flow 23 (2002) 678.
[50] J. Jiménez, J.C. DelÁdamo, O. Flores, The large-scale dynamics of near-wall turbulence, J. Fluid Mech. 505 (2004) 179.
[51] D. Poggi, A. Porporato, L. Ridolfi, An experimental contribution to near-wall measurements by means of special laser Doppler anemometry technique, Exp. Fluid 32 (2002) 366.
[52] L. Lyons, T.J. Hanratty, J.B. McLaughlin, Direct numerical simulation of passive heat transfer in a turbulent channel flow, Int. J. Heat Mass Transfer 34 (4) (1991) 1149.
[53] T. Wei, W.W. Willmarth, Reynolds-number effects on the structure of a turbulent channel flow, J. Fluid Mech. 204 (1989) 57.
[54] N.N. Mansour, J. Kim, P. Moin, Reynolds-stress and dissipation-rate budgets in a turbulent channel flow, J. Fluid Mech. 194 (1988) 15.
[55] B.C. Khoo, Y.T. Chew, C.J. Teo, Near-wall hot-wire measurements, Part II: Turbulence time scale, convective velocity and spectra in the viscous sublayer, Exp. Fluid 31 (2001) 494.
[56] R.D. Moser, J. Kim, N.N. Mansour, Direct numerical simulation of a turbulent channel flow up to $Re_\tau = 590$, Phys. Fluids 11 (1999) 943.
[57] J. Pallares, F.X. Grau, Frequency response of an electrochemical probe to the wall shear stress fluctuations of turbulent channel flow, Int. J. Heat Mass Transfer 51 (2008) 4753.
[58] T. Tsukahara, Y. Seki, H. Kawamura, D. Tochio, DNS of turbulent channel flow at very low Reynolds numbers, in: Proc. Fourth Int. Symp. on Turbulence and Shear Flow Phenomena, Williamsburg, USA, June 2005, p. 935.
[59] R.W. Smith, Effect of Reynolds number on the structure of turbulent boundary layers, Ph.D. thesis, Department of Mechanical and Aerospace Engineering, Princeton University, 1994.
[60] A.A. Townsend, Equilibrium layers and wall turbulence, J. Fluid Mech. 11 (1961) 97.
[61] A.N. Kolmogorov, The local structure of turbulence in incompressible viscous fluid for very large Reynolds number, Acad. Sci. 30 (1941) 301.
[62] S.B. Pope, Turbulent Flows, Cambridge University Press, 2000.
[63] R. Rubinstein, W.J.T. Bos, On the unsteady behavior of turbulence models, Phys. Fluids 21 (2009) 041701.
[64] M.H. Buschmann, M. Gad-el-Hak, Kolmogorov scaling of turbulent flow in the vicinity of the wall, Phys. D: Nonlinear Phenom. 239 (2010) 1288.
[65] Z.W. Hu, C.L. Morfey, N.D. Sandham, Wall pressure and shear stress spectra from direct simulations of channel flow, AIAA J. 44 (2006) 1541.
[66] J. Kim, P. Moin, R.D. Moser, Turbulence statistics in fully developed channel flow at low Reynolds number, J. Fluid Mech. 177 (1987) 133.